REMOTE SENSING TECHNOLOGIES FOR POST-EARTHQUAKE DAMAGE ASSESSMENT:
A CASE STUDY ON THE 2016 KUMAMOTO EARTHQUAKE

Fumio YAMAZAKI and Wen LIU

ABSTRACT: In the recent years, remote sensing technologies become important tools in disaster management, especially in the aftermath of destructive natural disasters. In this paper, various remote sensing data acquired after the M_w7.0 Kumamoto earthquake, Japan are introduced. Airborne optical and Lidar data as well as satellite optical and SAR data were captured by various international space agencies and aerial survey companies. Preliminary research results using these remote sensing data are demonstrated, comparing with the data from field surveys and GNSS observation, and seismic records.

KEYWORDS: remote sensing; the 2016 Kumamoto earthquake; UAV; damage distribution; surface rupture

1. INTRODUCTION

When a large-scale natural disaster strikes, information gathering for the affected area is often hindered by the disruption of road networks and telecommunication systems. In this situation, remote sensing technologies have been employed to assess the extent and degree of various damages (Yamazaki and Matsuoka 2007; Eguchi et al. 2008). There are mainly two categories of remote sensing from the sensor type: passive (optical and thermal sensors) and active (mainly radar sensors) remote sensing. Optical satellite systems work in the daytime and cannot observe objects under cloud-cover conditions. However, a radar system as Synthetic Aperture Radar (SAR) overcomes this problem and has been used in all day and all weather conditions (Dell'Acqua and Gamba 2012).

Various high-resolution optical and SAR satellites have been in operation in the last decade and they were employed to observe affected areas after major natural disasters, such as the 2011 Tohoku, Japan, earthquake and tsunami (Yague-Martinez et al. 2012; Liu et al. 2013), the 2011 central Thailand flood (Nakmuenwai and Yamazaki 2014), the 2013 Haiyan, Philippines typhoon (Mas et al. 2015), and the 2015 Gorkha, Nepal earthquake (Yamazaki et al. 2016). The acquired satellite data provided the information on inaccessible affected areas and they were used in emergency response activities.

Various aerial surveying technologies have also been developed in the last few decades, such as digital aerial cameras, Lidar (Light Detection And Ranging), and more recently, unmanned aerial vehicles (UAVs, drones). The images acquired by digital aerial cameras have much higher radiometric resolution than those from scanned analogue-camera photos, and thus they have been used in observing recent natural disasters (Yamazaki et al. 2008). Lidar is the most costly but the most accurate method to acquire digital surface models (DSMs) of the earth surface, and hence it has been used to develop detailed digital elevation models (DEMs) and 3D configuration of buildings (Vu et al. 2009).

UAVs have been used in recent decades for several civilian purposes, such as pesticide spraying, inspection of infrastructures such as bridges and towers, reconnaissance of hazardous areas (Nonami et al. 2010). Together with a 3D model construction technique called SfM (Structure-from-Motion), video footages from UAVs were used to depict the damage situation of affected buildings in Bologna, Italy (Fernandez et al. 2015) and that of affected urban areas due the 2015 Gorkha, Nepal earthquake (Yamazaki et al. 2015). The schematic figure of these platforms and sensors is shown in **Figure 1**.

In this paper, the use of various new remote sensing technologies employed in the 2016 Kumamoto, Japan earthquake are introduced. Preliminary research results using these remote sensing data are demonstrated, comparing with the data from field surveys and GNSS (Global Navigation Satellite System) observation, and seismic records.
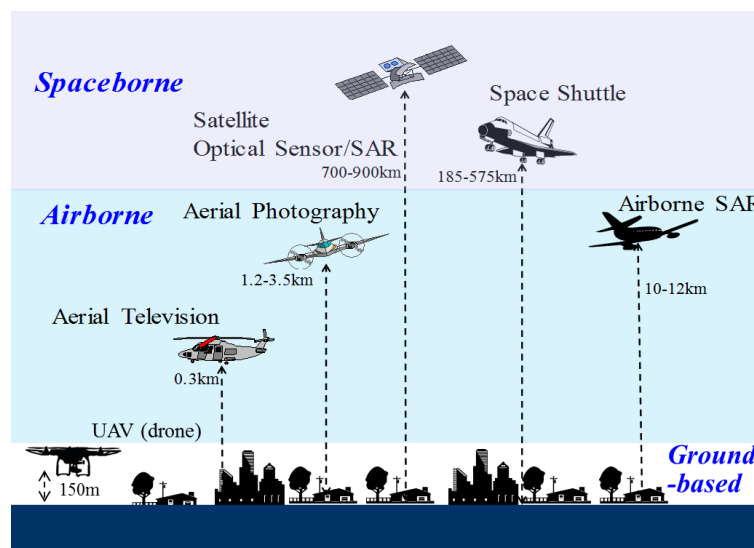
Figure 1. Various platforms and sensors used for remote sensing

2. THE 2016 KUMAMOTO EARTHQUAKE SEQUENCE

A $M_w6.2$ earthquake hit the Kumamoto prefecture in Kyushu Island, Japan on April 14, 2016 at 21:26 (JST). A considerable amount of structural damages and human casualties had been reported, including 9 deaths (Cabinet Office of Japan 2016). The epicenter was located at the end of the Hinagu fault with a shallow depth.

On April 16, 2016 at 01:25 (JST), about 28 hours after the first event, another earthquake of $M_w7.0$ occurred in the Futagawa fault, closely located with the Hinagu fault. Thus the first event was designated as the "foreshock" and the second one as the "mainshock". The epicenters of the both events were located in Mashiki town (about 33 thousand-population), to the east of Kumamoto city (about 735 thousand-population). Many aftershocks followed these events, and the total number of aftershocks (larger than magnitude 3.5) reached 264 times as of July 19, three months after the foreshock. This number is the largest among recent inland (crustal) earthquakes in Japan (Japan Meteorological Agency 2016).

Figure 2 shows the location of these causative faults and Japanese national GNSS Earth Observation Network System (GEONET) stations in the source area (Geospatial Information Authority of Japan (GSI) 2016). Note that the GEONET system has about 1,300 stations covering Japan's territory uniformly. The displacement of 75 cm to the east northeast (ENE) was observed at the Kumamoto station while that of 97 cm to the southwest (SE) was recorded at the Choyo station during the $M_w7.0$ mainshock. These observations validated the right-lateral strike-slip mechanism of the Futagawa fault.
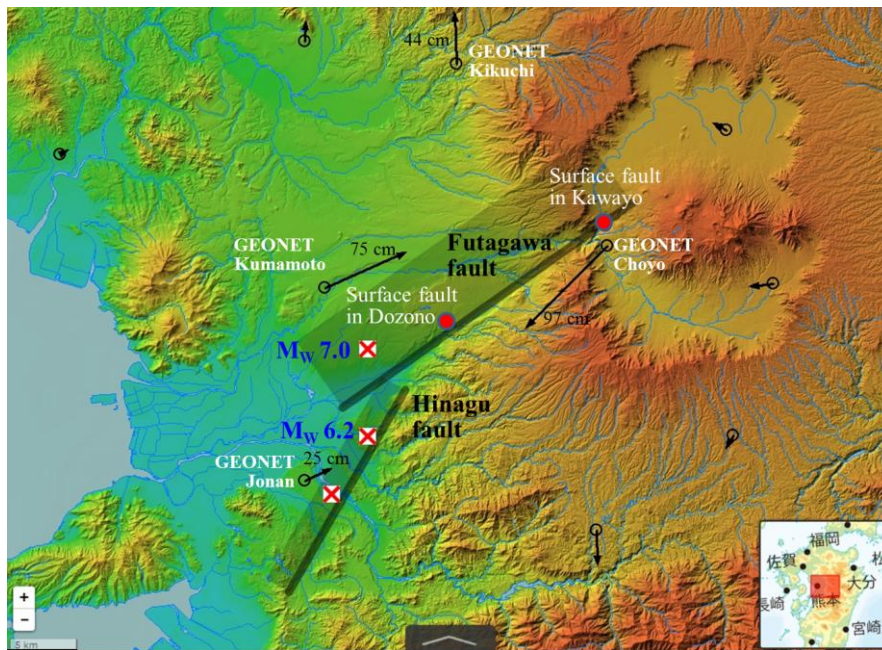
Figure 2. Epicenters, causative faults, and GEONET stations in the source zone of the 2016 Kumamoto, Japan earthquake

3. OBSERVATION IN FIELD SURVEYS

Extensive impacts due to strong shaking and landslides were associated by the Kumamoto earthquake sequence, such as collapse of buildings and bridges, and suspension of road and railway networks. A total of forty-nine (49) deaths and one missing were accounted by the earthquake sequence, mostly due to the collapse of wooden houses in Mashiki town and landslides in Minami-Aso village.

The first author has carried out field investigation of the affected areas three times: April 15 to 17 (experienced the mainshock in Kumamoto city), June 6 and 7, and July 3 and 4. **Figure 3** shows the route and visited sites in the field survey on June 6 and 7. **Figure 4** shows a surface rupture observed at the Dozono district in Mashiki town and the largest landslide observed at the Kawayo district in Minami-Aso village. The Aso-Ohashi bridge with 206-m span and 8-m width fell into the Kurokawa river by this landslide.

Figure 5 shows the damage situation of buildings in Mashiki town (a) and Kumamoto city (b). In Mashiki town, the peak ground acceleration (PGA) observed at the KiK-net Mashiki

(KMMH16) station was 925 cm/s^2 in the foreshock and 1,314 cm/s^2 in the mainshock. Due to the repeated very strong shocks, a large number of buildings were collapsed or severely damage, as show in the figure.

In Kumamoto city, the PGA at K-NET Kumamoto (KMM006) station, which is located in the eastern part of the city, was 580 cm/s^2 in the foreshock and 843 cm/s^2 in the mainshock. As seen in the photos, historical Kumamoto castle was severely damaged to its stone walls/foundations and roof-tiles. Some RC buildings suffered from structural and/or non-structural damage, but the most buildings in the city had minor or no damage.

Figure 3. Route and visited sites in the author's field survey on June 6 and 7, 2016

Figure 4. Surface rupture observed in Dozono district, Mashiki town (left) and the largest landslide observed from the Kawayo district, Minami-Aso village (right)

(a) Mashiki town: wooden house (left) and steel-frame (right)

(b) Kumamoto city: Iidamaru tower of Kumamoto castele (left) and RC building (right)

Figure 5. Damage situation of buildings in Mashiki town (a) and Kumamoto city (b)

4. SAR AND OPTICAL SATELLITE IMAGERY DATA

Soon after the occurrence of the first event, JAXA (Japan Aerospace Exploration Agency) carried out intensive monitoring of the source area using PALSAR-2 sensor onboard ALOS-2 satellite. **Figure 6** shows a result of Interferometric SAR (InSAR) analysis using a pair of PALSAR-2 data acquired on pre-event (2016/03/07) and post-mainshock (2016/04/18) times (GSI 2016).
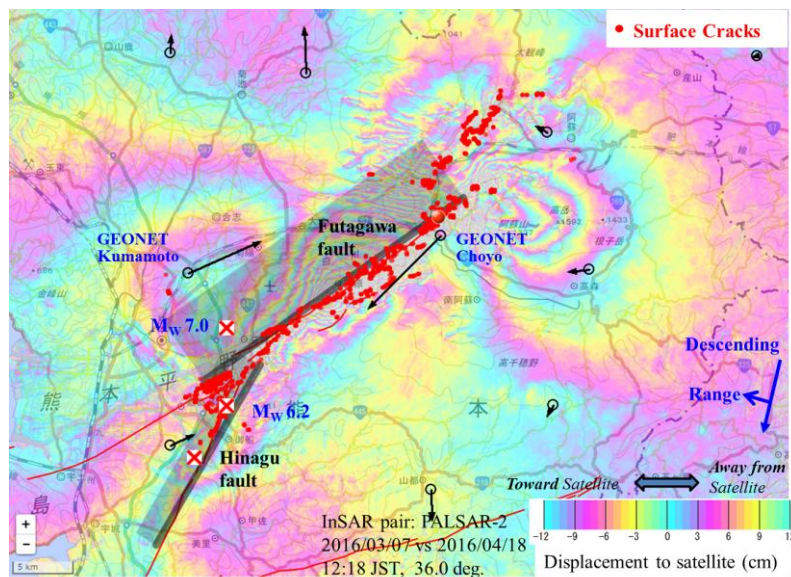
Figure 6. Result of InSAR analysis using a pair of PALSAR-2 data by GSI (2016)

Dense fringes, showing the relative displacement between the two time-instants toward the satellite direction, can be observed along the Futagawa fault line. Surface cracks, representing surface faulting and local soil displacements observed by aerial photo-interpretation (GSI 2016), are also plotted by red circles in the figure.

Using the pre-event PALSAR-2 pair (2015/11/30, 2016/03/07) data and the co-event PALSAR-2 pair (2016/03/07, 2016/04/18) data, the present authors calculated the spatial coherence values. **Figure 7** shows the color-composite of the pre-event and co-event coherence values, in which red color indicates the change of SAR backscatter in the co-event pair. Extensive landslides and severe building-damage areas along the fault line are clearly highlighted in the figure.
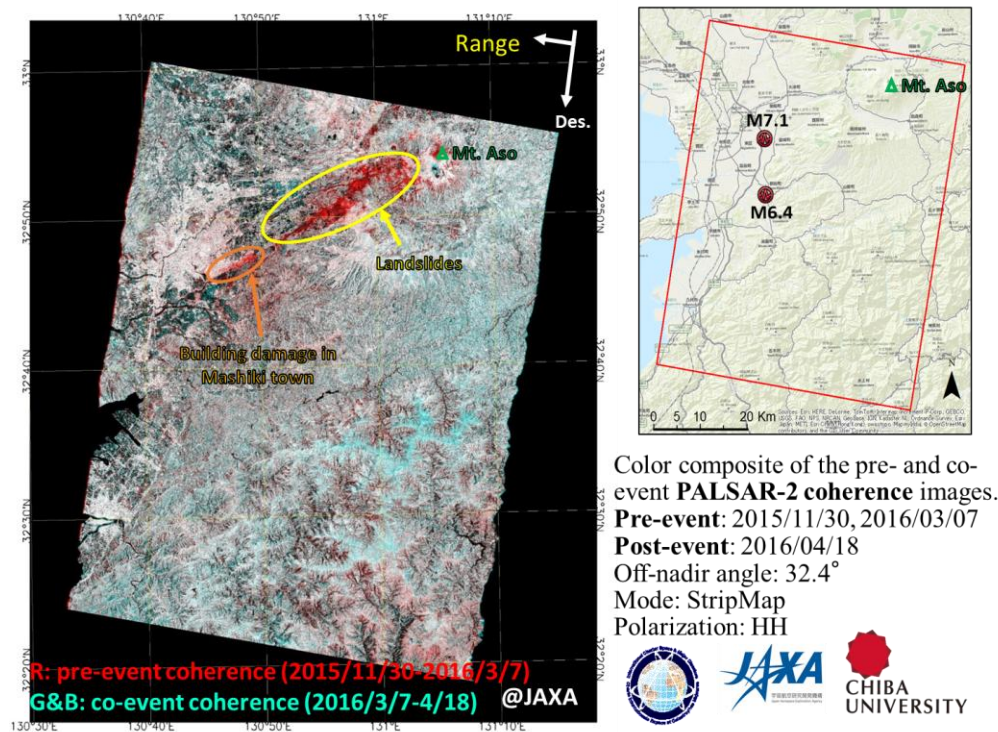
Figure 7. Color-composite of the pre- and co-event coherence values of PALSAR-2 data.

An international cooperation scheme for responding major natural disaster was activated soon after the foreshock of the Kumamoto earthquake based on the request of the Cabinet office of Japan (International Charter: Space and Major Disasters 2016). **Figure 8** shows one of the outputs of satellite data analysis which the present authors' group provided to the Space Charter. The figure compares the close-ups of high-resolution optical satellite images for an evacuation shelter in Mashiki town. In this event, a lot of residents in the affected area evacuated to shelters, designated by the local governments. The gymnasiums of public schools and facilities were assigned as shelters, which is the common practice in Japan. Since most people evacuated by car in the rural areas, the number of cars parking on the school ground could be a good estimate for the number of evacuees. In this school, the ground was seen to be full of evacuee's cars for a few days after the mainshock.
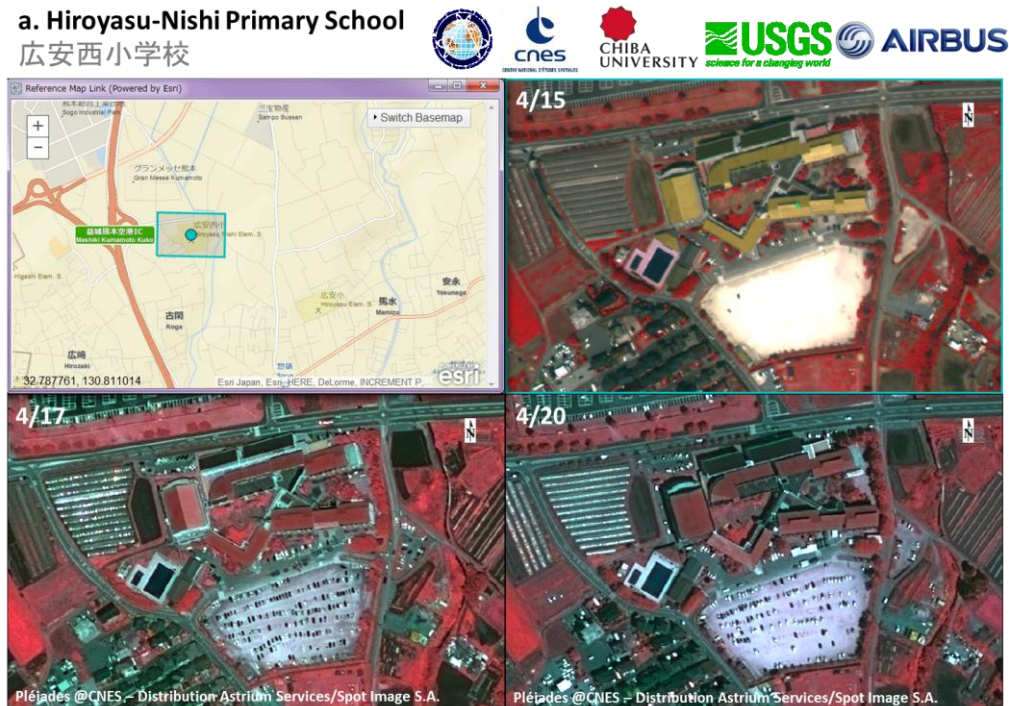
Figure 8. Comparison of close-ups of VHR optical satellite images for an evacuation site in Mashiki town, produced by Chiba University and provided to the Space Charter.

$$\Delta_{NDVI} = NDVI_{post} - NDVI_{pre}$$
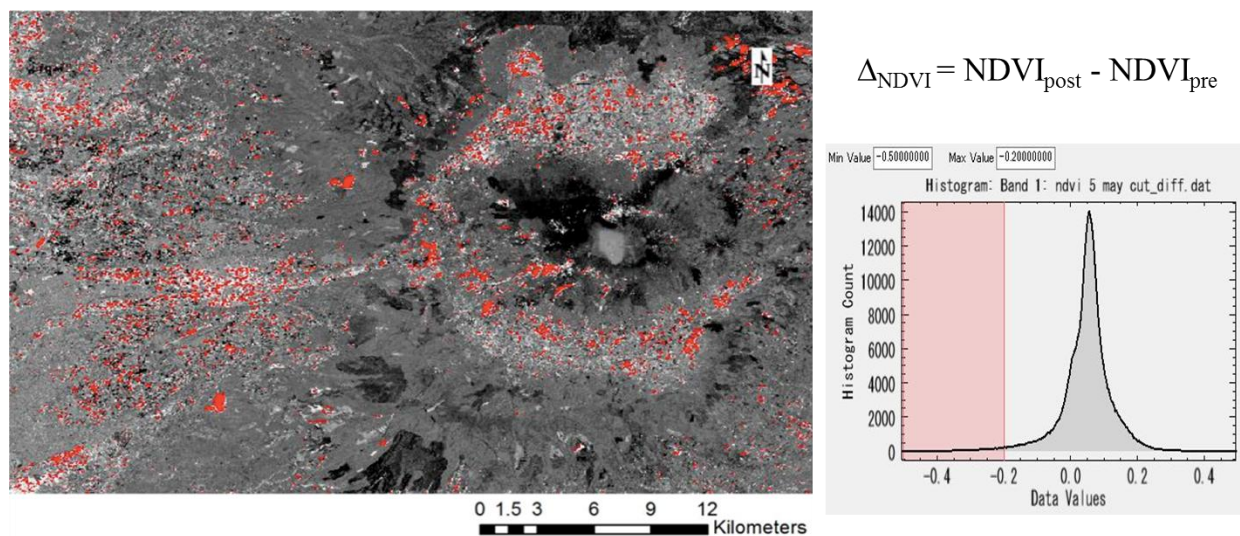
Figure 9. Extraction of landslides by the difference of NDVI values from Lansat-8 images

In order to grasp the locations of large scale landslides, moderate-resolution optical satellite images are useful, as demonstrated in case of the 2015 Gorkha earthquake (Tsuchida et al. 2015). For the Kumamoto earthquake, pre-event (2015/05/05) and post-event (2016/5/23) Landsat-8 images were used to extract pixels (15-m square after pan-sharpening), whose surfaces changed from vegetation to soil. The Normalized Difference Vegetation Index (NDVI) was employed to extract vegetated areas by the following equation:

$$NDVI = (NIR - R) / (NIR + R) \tag{1}$$

where R and NIR are the reflectance of the red and near-infrared bands, respectively. The NDVI is a simple and reliable index to identify the existence of vegetation, and therefore widely applied to assess the characteristics of the earth surface (Kouchi and Yamazaki 2007). **Figure 9** shows the difference of the pre- and post-event NDVI values for the Kumamoto area. The removal of vegetation by landslides, represented by the reduction of NDVI values, can be observed extensively along the fault line and around the outer rim of Mt. Aso's cardera.

5. AERIAL PHOTOGRAPHS AND LIDAR DATA

From the next morning of the foreshock, a lot of aerial surveying flights were carried out by government agencies and aerial survey companies in Japan. **Figure 10** shows vertical aerial photo shooing points (blue dots) conducted by the Geospatial Information Authority of Japan (GSI) on April 16, 2016 (the day of the mainshock). Many aerial photos were also acquired by GSI on April 15 (after the foreshock) and days after the mainshock.

Orthorectified images were produced from them and all the imagery data have been uploaded on the GSI's web map server (http://maps.gsi.go.jp/). **Figure 11** shows an example of orthorectified photos, over the Dozono district in Mashiki town. The surface faulting shown in **Figure 2** can be observed as well as landslides and collapsed buildings.

Oblique photos were also acquired by GSI at several locations including major damage situations. **Figure 12** shows the photos including collapsed buildings in Mashiki town (on April 15) and the largest landslide in Minami-Aso village (on April 16). These oblique photos can characterize the damage situations well since the 3D information is included.
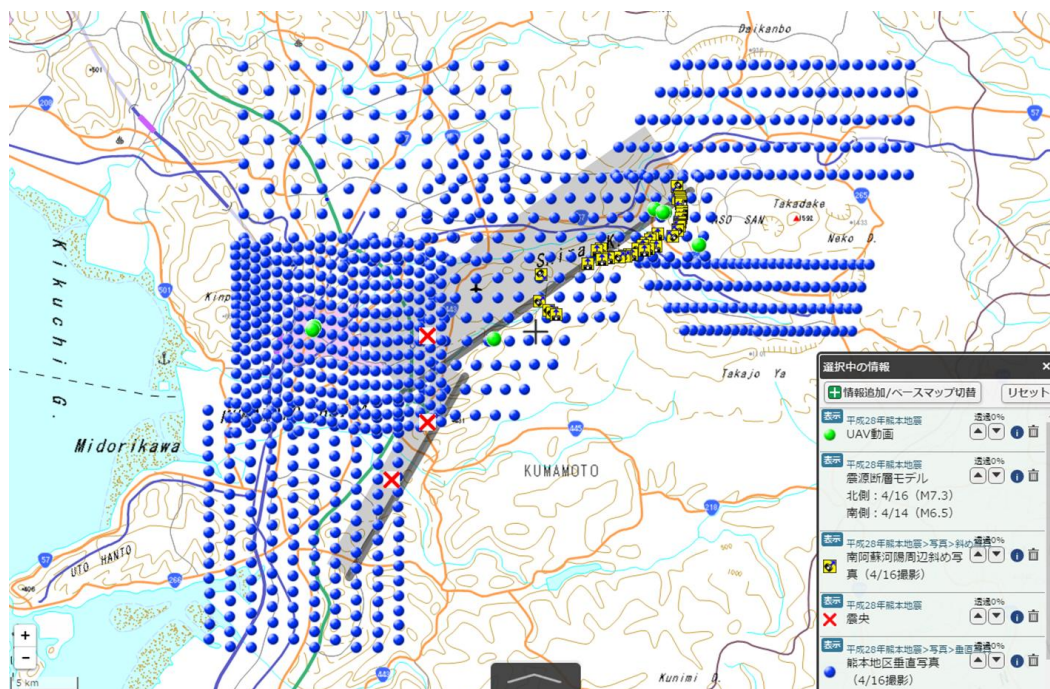
Figure 10. Map showing vertical aerial photo shooing points (blue dots), oblique photo shooting points (yellow symbols), and UAV flights (green points) conducted by GSI

Figure 11. Orthorectified photo taken on April 16 by GSI over Dozono district. The surface faulting shown in Figure 2 and several landslides can be recognized.

Figure 12. Oblique photos including collapsed buildings in Mashiki town (left, on April 15) and the largest landslide in Minami-Aso village (right, April 16) taken by GSI (2016).

Lidar surveys were also carried out for the affected areas by the GSI and some air survey companies. Among them, Asia Air Survey Co., Ltd. (2016) collected Lidar data with the density of 1.5~2 points/m^2 just after the first (April 14) earthquake, on April 15. A second mission to acquire Lidar data was dispatched on April 23, which could obtain the data with 3-4 points/m^2 density. This Lidar pair dataset is one of the few cases in which pre- and post-event digital surface models (DSMs) were obtained from the same airplane, instrument, and pilot (Air Survey Co., Ltd. 2016).

The spatial correlation coefficient of the two Lidar data was calculated using a 101 x 101 pixels window, as described in our companion paper (Moya et al. 2016). The location of the maximum value relative to the center of the window is two pixels (100 cm) to the west and one pixel (50 cm) to the south, which is consistent with the displacement time history calculated from the double integration of acceleration records. **Figure 13** shows the detected horizontal (arrow) and vertical (color) displacements between the two Lidar data (a) and the enlargement around Mishiki town hall (b), in which red color corresponds to the settlements due to building collapse.
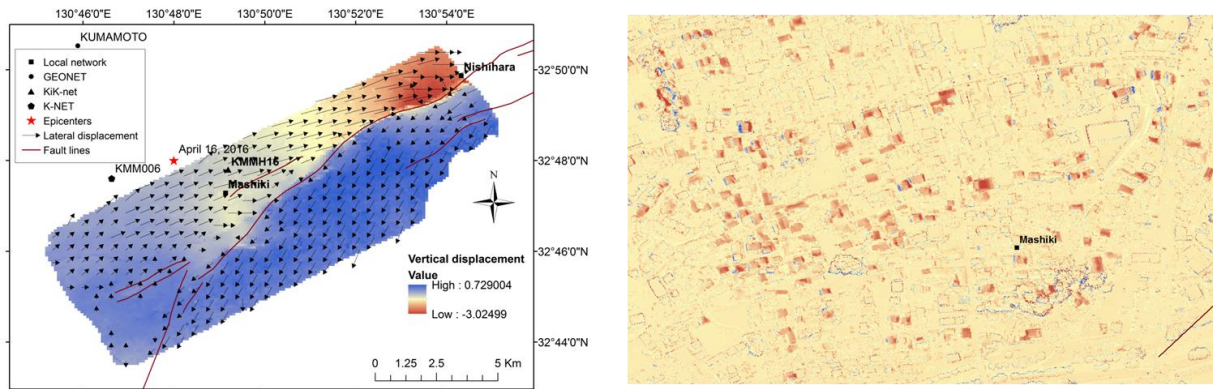
(a) Crustal movement estimated from Lidar data   (b) enlargement around Mishiki town hall

Figure 13. Detected horizontal (arrow) and vertical (color) displacements between the two Lidar data (a) and its enlargement around Mishiki town hall (b)

6. UAV VIDEO SHOOTING AND 3D MODEL CONSTRUCTION

The use of drones has been expanded from professional to personal purposes in the last few years. But some inconvenient incidents occurred in USA and Japan in 2015, and the laws and regulations for drones have been issued in several countries including Japan (Ministry of Land, Infrastructure, Transport and Tourism of Japan (MLIT) 2015). After the Kumamoto earthquake under this situation, several UAV fights were conducted out outside of restricted areas (such as Densely Inhabited Districts: DIDs) and inside restricted areas with the permission by the Civil Aviation Bureau of MLIT.

The GSI engaged in video shooting over disaster affected sites in Kumamoto prefecture, such as the Kumamoto castle and collapsed Aso-Osashi bridge. Using these video footages, the authors' group produced 3D models as shown in **Figure 14**. In the figure, the developed 3D model (left) of the Iidamaru tower of the Kumamoto castle and the estimated camera positions (right) of the snapshots used in the SfM (Structure-from-Motion) technique are presented. In the study, the Agisoft's *PhotoScan* software was used for 3D model construction.
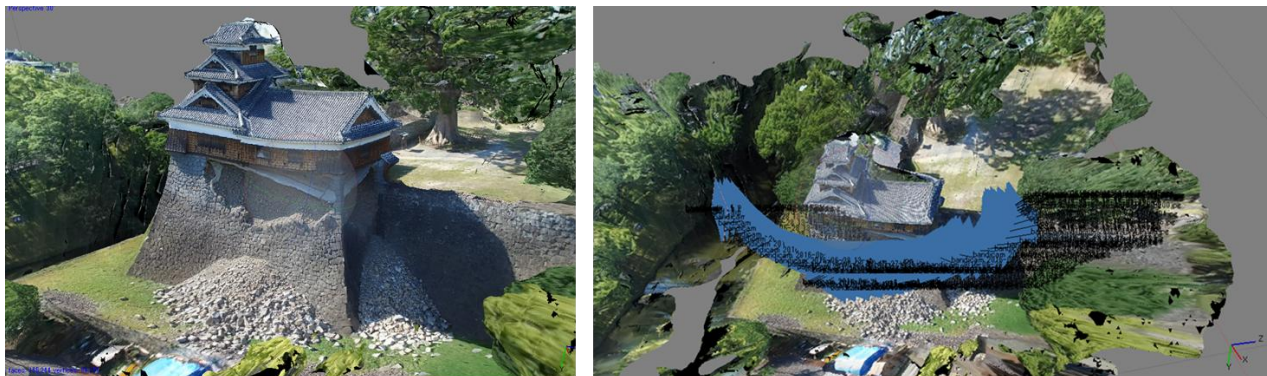
Figure 14. Developed 3D model of the Iidamaru tower of the Kumamoto castle (left) and the estimated camera positions of the snapshots used in the SfM (right, blue squares)

7. CONCLUSIONS

Importance of remote sensing technologies in disaster management is increasing due to the advancement of various spaceborne/airborne platforms and sensors. In this paper, various remote sensing data acquired after the $M_w7.0$ Kumamoto earthquake, Japan were introduced. Satellite SAR sensors, notably PALSAR-2, observed affected areas before and after the earthquake sequence and the acquired data were used to evaluate crustal movements and landslides. Optical satellites also observed the affected areas under the framework of the international space charter. Lidar missions as well as photo- and video-shootings from airplanes and UAVs were carried out by government agencies and air survey companies in Japan. Digital surface models (DSMs) and 3D structure models were developed from these aerial data, together with georeferenced photographic images. Preliminary research results on the earthquake effects using these remote sensing data were demonstrated, and they were compared with the data from field surveys and GNSS observation, and seismic records.

REFERENCES

Asia Air Survey Co., Ltd. (2016) the 2016 Kumamoto Earthquake.
http://www.ajiko.co.jp/en/blog/y2016/id572751JWX/

Geospatial Information Authority of Japan (2016) the 2016 Kumamoto Earthquake.
http://www.gsi.go.jp/BOUSAI/H27-kumamoto-earthquake-index.html

Cabinet Office of Japan (2016) Summary of damage situation in the Kumamoto earthquake sequence,
http://www.bousai.go.jp/updates/h280414jishin/index.html

Dell'Acqua, F. and Gamba, P. (2012) Remote sensing and earthquake damage assessment: Experiences, limits, and perspectives. **Proceedings of the IEEE** 100 (10), 2876-2890.

Fernandez Galarreta, J., Kerle, N., & Gerke, M. (2015) UAV-based urban structural damage assessment using object-based image analysis and semantic reasoning, **Natural Hazards and Earth System Sciences**, 15. 1087–1101.

Eguchi, R.T., Huyck, C., Ghosh, S., Adams, B.J. (2008) The application of remote sensing technologies for disaster management. **The 14th World Conference on Earthquake Engineering**, CD-ROM.

Kouchi, K., and Yamazaki, F. (2007) Characteristics of tsunami-affected areas in moderate-resolution satellite images. **Transactions on Geoscience and Remote Sensing**, IEEE, Vol. 45, No. 6, 1650-1657.

International Charter: Space and Major Disasters (2016) Earthquake in Japan
https://www.disasterscharter.org/web/guest/-/earthquake-in-jap-1

Japan Meteorological Agency (2016) The number of aftershocks of recent inland earthquakes in Japan.
http://www.data.jma.go.jp/svd/eqev/data/2016_04_14_kumamoto/kaidan.pdf

Liu, W., Yamazaki, F., Gokon, H., and Koshimura, S. (2013) Extraction of tsunami-flooded areas and damaged buildings in the 2011 Tohoku-Oki Earthquake from TerraSAR-X intensity images. **Earthquake Spectra**, 29(S1), S183-S200.

Mas, E., Bricker, J., Kure, S., Adriano, B., Yi, C., Suppasri, A., Koshimura, S. (2015) Field survey report and satellite image interpretation of the 2013 Super Typhoon Haiyan in the Philippines. **Natural Hazards and Earth System Sciences**, 15, 805–816.

Minister of Land, Infrastructure, Transport and Tourism of Japan (2015). Japan's safety rules on Unmanned Aircraft (UA). http://www.mlit.go.jp/en/koku/uas.html

Moya, L, Yamazaki, F., Liu, W., Chiba, T. (2016) Estimation of coseismic displacement in the 2016 Kumamoto earthquake from Lidar data. **6th ASIA Conference on Earthquake Engineering**, Cebu City, Philippines.

Nakmuenwai, P., Yamazaki, F. (2014) Extraction of flooded areas in the 2011 Thailand flood from RADARSAT-2 and ThaiChote images. **Proceedings of the IEEE 2014 International Geoscience and Remote Sensing Symposium**, Quebec, Canada, 3354-3357.

Nonami, K., Kendoul, F., Suzuki, S., Wang, W., and Nakazawa, D. (2010) **Autonomous flying robots**, Springer, Tokyo, doi:10.1007/978-4-431-53856-1.

Tsuchida, R., Liu, W., and Yamazaki, F. (2015) Detection of landslides in the 2015 Gorkha, Nepal earthquake using satellite imagery. **Proc. 36th Asian Conference on Remote Sensing**, Manila, Philippines, 10p.

Vu, T. T., Yamazaki, F. and Matsuoka, M. (2009) Multi-scale solution for building extraction from LiDAR and image data. **International Journal of Applied Earth Observation and Geoinformation,** 11, 281–289.

Yague-Martinez, N., Eineder, M., Cong, X.Y., and Minet, C. (2012) Ground Displacement Measurement by TerraSAR-X Image Correlation. The 2011 Tohoku-Oki Earthquake, **IEEE Geoscience and Remote Sensing Letters**, Vol. 9, No. 4, 539-543.

Yamazaki, F. and Matsuoka, M. (2007) Remote Sensing Technologies in Post-Disaster Damage Assessment. **Journal of Earthquakes and Tsunamis**, Vol. 1, No. 3, pp. 193-210.

Yamazaki, F., Suzuki, D. and Maruyama, Y. (2008) Use of digital aerial images to detect damages due to earthquakes. **Proc. 14th World Conf. Earthquake Engineering**, Paper No. 01-1049, CD-ROM, 8 pp.

Yamazaki, F., Matsuda, T., Denda, S. and Liu, W. (2015) Construction of 3D models of buildings damaged by earthquakes using UAV aerial images. **Proc. of the Ninth Pacific Conference on Earthquake Engineering**, Sydney, Australia, Paper No. 204, 8p.

Yamazaki, F., Bahri, R., Liu, W., Sasagawa, T. (2016) Damage extraction of buildings in the 2015 Gorkha, Nepal earthquake from high-resolution SAR data, **Proc. of SPIE**, Vol. 9877, 98772K-1-11, doi: 10.1117/12.2223306.

ABOUT THE AUTHORS

Fumio Yamazaki is a professor at the Department of Urban Environment Systems, Chiba University, Japan. Email: fumio.yamazaki@faculty.chiba-u.jp

Wen Liu is an assistant professor at the Department of Urban Environment Systems, Chiba University, Japan. Email: wen.liu@chiba-u.jp

ACKNOWLEDGEMENTS